To study the surface flux distribution of the Moon by astrophotography from National Observatory, Nagarkot, Nepal

Janak Ratna Malla*, Madan Aryal*, Saroj Raj Shahi, Walter Saurer***and Binil Aryal******

*Department of Physics, Amrit Campus, Thamel, Tribhuvan University, Nepal.

**B.P. Koirala Memorial Planetarium, Observatory and Science Museum Development Board, Kathmandu, Nepal.

***Institute of Astro-particle Physics, Innsbruck University, Austria.

****Central Department of Physics, Kirtipur, Kathmandu, Tribhuvan University, Nepal.

Abstract: We studied visual flux collected by Meade 16-inch LX200GPS Schmidt-Cassegrain telescope in between April and June, 2025 from the National Observatory Nagarkot, Nepal. The goal of this study was to use these data and analyze to gain important understanding and study of visual flux emitted from the outer layers of the Moon. Five lines through the center were drawn in the figure joining the innermost contour and variation of relative flux density along these five lines were calculated and studied. The result showed that there was consistent decrease in the relative flux distribution from inner to outer region of the Moon. When we move more towards the outer region, the relative flux distribution decreases slowly and it reaches close to the background flux density value when we reached the outermost region. The average background radiation (F_B), from our calculation, was found to be 59.98 P.U. (Pixel Units). And, the relative flux density per pixel was found to be in the range of -0.98 to -41.98 with background subtraction. From our calculation, the relative flux density of the Moon was found to be in negative values, which indicates that the Moon is one of the brightest objects in the night sky.

Keywords: Astrophotography; Surface flux density; Craters; Lunar.

Introduction

Observational astronomy concerned with the study, gatheringand recording of data on celestial objects using telescopes and other astronomical instruments. Astrophotography is a specialized photography technique that focuses on photographing celestial objects and other astronomical phenomena. Besides being able to record the details of extended objects such as the Moon, Sun, and planets, astrophotography has the ability to image objects invisible to the human eye such as dim stars, nebulae, and galaxies. This is done by long time exposure since both film and digital cameras can accumulate and sum light photons over these long periods of time. Earth's only natural satellite is simply called "the moon" because people didn't know other moons existed until Galileo Galilei discovered four moons orbiting Jupiter in 1610[1].This brightest and largest object in our night sky, makes Earth a more livable planet by moderating our home planet’s wobble on its axis, leading to a relatively stable climate. It also causes tides, creating a rhythm that

Author for correspondence: Janak Ratna Malla, Department of Physics, Amrit Campus, Thamel, Tribhuvan University, Nepal.
Email: janakmalla@ac.tu.edu.np; https://orcid.org/0000-0002-9035-1378
Received: 16 Apr, 2026; Received in revised form: 13 May, 2026; Accepted: 20 May, 2026.
Doi: https://doi.org/10.3126/sw.v19i19.96474

has guided humans for thousands of years. The moon was likely formed after a Mars-sized body collided with Earth.

It is important to note that the terms "Near side" and "Far side" can be little deceptive because they're relative to Earth's perspective. The moon is tidally locked to Earth, which means that it always presents the same face to our planet as it orbits it. So, from the moon's perspective, the near side is the side facing Earth, and the far side is the side facing away. Before the Soviet Luna-3 Spacecraft took the first pictures of it in 1959, the far side of the moon was mainly unknown and unexplored. But, in April 6, 2026, first flyby pictures of moon captured by ArtemisII (4 Astronauts). Its geological features set it apart from the neighboring side, including a rougher, more extensively cratered landscape and less maria[2-5].

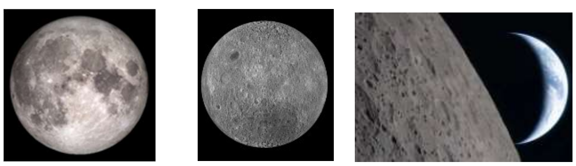

Figure 1: The Near side (left) and the Far side (right) of the Moon.

Table 1: Facts of the Moon[4].

Mass	7.35 x 10^{22} kg
Density	3.34 gm cm^{-3}
Diameter	3,476 Km
Average Distance from Earth	384,400 Km
Period of Revolution(Sidereal)	27.3 Earth Days(Relative to Stars)
Period of Revolution(Synodic)	29.5 Earth Days(Relative to Earth)
Orbital Velocity	1.08 Km s^{-1}
Escape Velocity	2.38 Km s^{-1}
Strength of gravity on the surface	1.7 NKg^{-1}
Maximum Distance from Earth(Apogee)	407,000 Km
Minimum Distance from Earth(Perigee)	356,000 Km
Albedo	0.07

Y. Shkuratov et al., 2011[5] researched optical studies of the Moon and their diagnostic significance, which included three interconnected parts: phase photometry, spectrophotometry, and polarimetry. Oberst et al., 2012[6] analyzed the statistics of impact craters in order to calculate the total meteoroid flux on the lunar surface. Forgan et al.,2014[7] explored about the surface flux patterns on Planets in circumbinary Systems. But, this work desires to achieve, Firstly, create a complete data-set of the Moon's surface flux density, F_T and the background count, F_B by cautiously capturing high-resolution images of the Moon with a Meade 16" LX200GPS optical telescope. Furthermore, this study hopes to contribute to the larger field of planetary science and astrophysics.

Craters

Craters Around 80% of the moon's surface is fascinated with craters. While The near Side shows the sparse distribution of Craters, seemingly dominated by Maria and Basins, The Far Side is highly populated with the Craters as large as 1000 Km in diameter. The word 'Crater' was first adopted by Galileo from the Latin word which means Cup when he viewed the lunar surface with his telescope in 1609 AD and concluded that the Moon in not a perfect sphere but it is fascinated with both mountains and depressions[8-11].

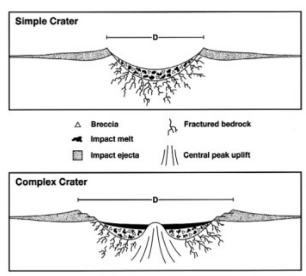

Figure 2: Simple and complex crater.

Observation AndSampling

The Observatory is equipped with Meade16"LX200 GPS Schmidt-Cassegrain Optical Telescope, for observation[12-15].

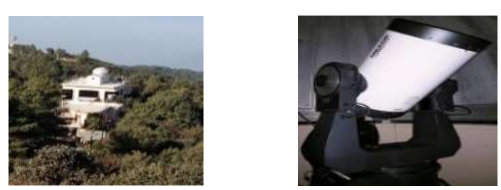

Figure 3: National Observatory, Nagarkot and Meade 16".

Table 2: Facts about telescope[16].

Optical Design	Schmidt−Cassegrain
Clear aperture	406.4 mm(16")
Focal Length	4064 mm
Focal ratio(Photographic Speed)	$f/10$
Resolving Power	0.28 arc-sec
Primary Mirror Diameter	415.9 mm (16.375")
Pointing Precision	2 arc-minutes in GO TO mode
Power	18V power supply
Net telescope weight	318 lbs

We visited the observatory in more than three times in different seasons. On 11^{th} and 12^{th} May, 2025, we were able to take few FITS images of the surface of the Near side of the Moon. During our observation, the presence of background noise reduced the effective image quality of FITS(Flexible image transport system) images. We noted theTimeat the time of our observations. Numbers of FITS images and JPEG images (Joint photographic experts group image) of the near side of the lunar surface were recorded starting from 8:00 PM to 10:00 PM.

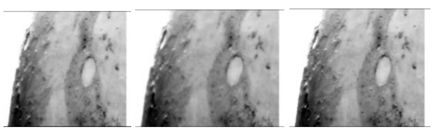

Figure 4: FITS images of the near side of the surface of Moon, observed by using Meade 16" LX200GPS Schmidt-Cassegrain Telescope, captured by using Meade LPI Camera, processed by AUTOSTAR II System, using different filters blue, red and green respectively (from left to right).

From figure 4, The FITS image is taken in a test to calculate the surface flux distribution of theMoon using the ALADIN2.5 and ORIGIN5.0 software.

Method and Data Analysis

In order to analyze the data to determine the flux radiated by the Moon's outer surface, we apply the following processes[17-19]

1. First of all, the near side of the surface of the Moon was observed through the eye-piece of Meade 16" LX200GPS Schmidt-Cassegrain Optical Telescope fitted in National Observatory, Nagarkot, Nepal.
2. The eye-piece was then replaced by LPI camera and FITS images as well as JPEG images of moon crater were captured using AUTOSTAR SUITE3.08 software.
3. Out of large number of images, the best FITS imageof the Moon with good surface structure andrelief was picked for further processing with ALADIN2.5.
4. Five lines were drawn through the center of the Moon to find the relative flux variation in every pixel along each lines using ALADIN2.5.
5. The data reduction software, ALADIN2.5was used to take a background count of relative fluxdensity,which was then used to correct the value of relative flux densities along each line.This background count was further used to rectify the relative flux densities in each quadrant in the outer region of the Moon.
6. Finally,the collected data were entered into ORIGIN5.0 software and a graph of Relative FluxDensity versus Pixel Number was plotted and evaluated.

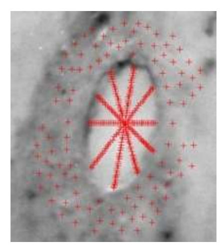

Figure 5: Calculation of background flux density. Each '+' sign represents the point where the data for background count is taken.

Relative flux density variation in the moon

Figure 6, shows the FITS image of the near side of the surface of the Moon along with five lines, Line-1, Line-2, Line-3, Line-4 and Line-5, drawn through the center with the help of ALADIN2.5 software. Tagging in each single pixel will record the flux density (**F_T**) along the Line-1.Each pixel's co-ordinate(X, Y) and flux (F_T) will be recorded. Similarly, we will repeat the process for Line-2, Line-3, Line-4and Line-5. The first click on the pixel is marked by 1, the second by 2, and so on down each line. F_T represents the flux density value of each pixel. The corrected value of flux density long each line is obtained by subtracting each F_T with the average background flux

Table 3: The table determining average background. First column is the Pixel Number (PN) of the points clicked in the background. Second and third column are co-ordinates of the corresponding point (X and Y co-ordinate), and fourth column corresponds to the flux density of those points called background flux, F_B.The other columns, fifth, sixth, seventh and eighth, are the continuation of the first, second, third and fourth columns respectively.

PN	X	Y	F_B	PN	X	Y	F_B
1	71.0	83.0	63.0	51	78.0	146.0	62.0
2	60.5	64.5	54.0	52	63.5	121.0	72.0
3	72.5	64.0	65.0	53	55.5	130.0	69.0
4	75.5	55.0	60.0	54	68.5	129.0	80.0
5	62.5	52.5	78.0	55	61.5	140.0	70.0
6	65.5	36.0	66.0	56	56.5	152.5	69.0
7	74.5	36.5	68.0	57	69.0	154.5	39.0
8	81.5	37.0	62.0	58	90.5	160.0	65.0
9	91.0	34.5	59.0	59	109.5	161.0	74.0
10	98.5	29.0	66.0	60	99.5	170.5	72.0
11	105.5	24.0	60.0	61	123.5	150.5	64.0
12	69.5	23.0	75.0	62	133.0	141.0	69.0
13	77.5	14.0	79.0	63	144.0	131.5	78.0
14	86.0	7.0	76.0	64	154.5	119.0	74.0
15	82.5	23.5	63.0	65	160.0	103.0	57.0
16	95.5	16.0	73.0	66	173.5	104.0	34.0
17	109.0	13.5	42.0	67	182.5	103.5	35.0
18	102.5	7.0	44.0	68	181.0	122.0	34.0
19	121.0	176.0	66.0	69	170.0	117.0	48.0
20	133.5	176.0	55.0	70	162.0	128.0	58.0
21	135.5	14.0	58.0	71	171.5	130.0	48.0
22	122.5	11.5	52.0	72	158.5	139.0	80.0
23	148.0	29.0	52.0	73	148.5	141.5	58.0
24	155.0	40.0	47.0	74	158.0	150.5	70.0
25	158.5	52.0	49.0	75	150.5	162.0	68.0
26	161.5	66.0	52.0	76	145.5	172.0	54.0
27	164.0	84.5	46.0	77	132.5	179.0	61.0
28	173.5	67.0	45.0	78	118.5	179.0	61.0
29	181.5	59.5	40.0	79	110.5	173.0	67.0
30	170.5	50.0	46.0	80	119.5	163.0	61.0
31	181.5	44.0	42.0	81	128.0	169.0	54.0
32	172.0	40.0	46.0	82	137.5	167.0	47.0
33	178.5	30.0	30.0	83	130.5	158.0	57.0
34	164.5	30.0	40.0	84	136.0	149.5	63.0
35	158.5	15.0	43.0	85	145.5	155.0	65.0
36	170.5	19.0	37.0	86	66.0	165.0	59.0

PN	X	Y	F_B	PN	X	Y	F_B
37	149.5	5.5	54.0	87	77.5	172.0	63.0
38	188.5	52.5	43.0	88	94.5	179.5	69.0
39	188.5	37.5	52.0	89	79.5	158.0	61.0
40	70.0	96.5	62.0	90	98.5	153.0	96.0
41	54	96.5	78.0	91	111.0	1.0	62.0
42	43.5	103.5	70.0	92	129.5	3.0	65.0
43	44.5	113.5	68.0	93	147.5	15.5	42.0
44	45.5	128.5	68.0	94	128.5	23.0	86.0
45	46.5	141.0	78.0	95	156.0	24.0	36.0
46	56.5	109.0	71.0	96	116.0	17.0	40.0
47	52.0	118.0	71.0	97	164.0	7.0	38.0
48	70.0	107.5	59.0	98	141.5	179.0	51.0
49	73.0	121.5	73.0	99	48.5	88.0	74.0
50	77.5	132.0	72.0	100	93.0	1.0	101.0

Average background flux, F_B = Average of fourth and eighth columns of Table 3=59.98 P.U (Pixel Units).

(F_B), i.e., $F_{TB} = F_T - F_B$. The corrected value is the actual emission of flux density.

Variation along Line-1

The variation of flux density along the Line-1 is shown in figure 7. The graph presents a scatter plot diagram of Relative Flux Density against Pixel Number with constant flux density for the inner region.

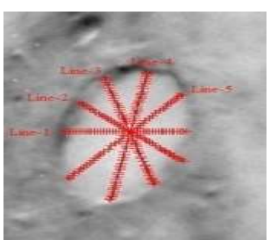

Figure 6: FITS image with flux density variation. Line-1, Line-2, Line-3, Line-4 and Line-5 are five lines drawn through the center of the FITS image using ALADIN2.5 software. Points are tagged along these lines and readings are obtained. These values are listed in the Tables 4.

This graph (Fig. 7) relates to the Table 4. The flux density is measured in each pixel of Line-1 from left to right. The graph shows that the relative flux density increases from outer region to the inner region, and then again decreases

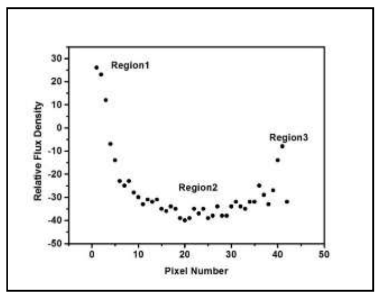

Figure 7: Variation of relative flux densityalong Line-1 of figure 6 of moon.

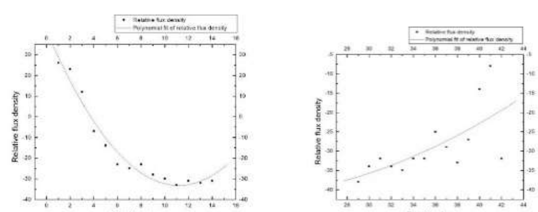

Figure 8: Flux density variation in region 1 along line- 1 of figure 6 of Moon (Left), Flux density variation in region 3 along line-1 with second degree polynomial fit (right).

moving towards the outer region. This is because of the brighter the object appears, the lower the value of its magnitude. The graph is divided into three regions: Region 1,2and3. Using the polynomial fit model $y = c + mx + ax^2$, the nature of the relationship between relative

Table 4: Variation of relative flux density with flux number. The first column lists the Pixel Number (PN). The second and the third column give the pixel co-ordinate (X, Y). The fourth column gives the corresponding flux density (F_T) of (X, Y) co-ordinate and the fifth column gives the flux density of corresponding pixels corrected with background flux, i.e. (F_{TB}). The other columns, sixth, seventh, eighth, ninth and tenth, are the continuation of the first, second, third, fourth and fifth columns respectively. This table represents the data of relative flux density along the Line-1 of figure 6.

PN	X	Y	F_T	F_{TB}	PN	X	Y	F_T	F_{TB}
1	90.0	84.0	86.0	26.02	22	122.0	84.0	25.0	-34.98
2	91.5	84.0	83.0	23.02	23	123.5	84.0	23.0	-36.98
3	92.5	84.0	72.0	12.02	24	124.5	84.0	25.0	-34.98
4	94.0	84.0	53.0	-6.98	25	126.0	84.0	21.0	-38.98
5	95.5	84.0	46.0	-13.98	26	127.5	84.0	22.0	-37.98
6	97.0	84.0	37.0	-22.98	27	128.5	84.0	26.0	-33.98
7	100.0	84.0	35.0	-24.98	28	129.5	84.0	22.0	-37.98
8	101.5	84.0	37.0	-22.98	29	130.5	84.0	22.0	-37.98
9	102.5	84.0	32.0	-27.98	30	132.0	84.0	26.0	-33.98
10	104.0	84.0	30.0	-29.98	31	133.5	84.0	28.0	-31.98
11	105.5	84.0	27.0	-32.98	32	135.0	84.0	26.0	-33.98
12	107.0	84.0	29.0	-30.98	33	136.5	84.0	25.0	-34.98
13	108.5	84.0	28.0	-31.98	34	138.5	84.0	28.0	-31.98
14	110.0	84.0	29.0	-30.98	35	140.0	84.0	28.0	-31.98
15	111.5	84.0	25.0	-34.98	36	98.5	84.0	35.0	-24.98
16	113.0	84.0	24.0	-35.98	37	142.5	84.0	31.0	-28.98
17	114.5	84.0	26.0	-33.98	38	144.0	84.0	27.0	-32.98
18	116.0	84.0	25.0	-34.98	39	145.5	84.0	33.0	-26.98
19	117.5	84.0	21.0	-38.98	40	147.0	84.0	46.0	-13.98
20	119.0	84.0	20.0	-39.98	41	148.5	84.0	52.0	-7.98
21	120.5	84.0	21.0	-38.98	42	137.0	84.0	28.0	-31.98

flux density and pixel number is determined. The curve fitting of relative flux density versus pixel number is presented by figure 8.

At region 1, the parabolic fit model is **y** = 41.73 – 13.43x + $0.601x^2$ with error 3.78, 1.16 and 0.075 in the parameter c, m and a respectively. Similarly, at region 3, the parabolic fit model is y = -33.93 – 1.07x + $0.034x^2$with error 156.97, 8.92 and 0.126 in the parameter c, m and a respectively.

Variation along Line-2, 3, 4 and 5

The variation of flux density along the Line-2, 3, 4 and5 are shown in figure 9. The graph presents a scatter plot diagram of Relative Flux Density against Pixel Number with constant flux density for the inner region.

The graph shows that the relative flux density increases from outer region to the inner region, and then again decreases moving towards the outer region. The graph is divided into three regions: Region 1, 2 and 3.

Using the polynomial fit model $y = c + mx + ax^2$, the nature of the relationship between relative flux density and pixel number is determined. The curve fitting of relative flux density versus pixel number is presented by figure 10. At region 1, Line2,3,4and 5, the parabolic fit model is **y** = 28.72 – 12.34x + $0.635x^2$ with error 5.15, 1.82 and 0.136 ,

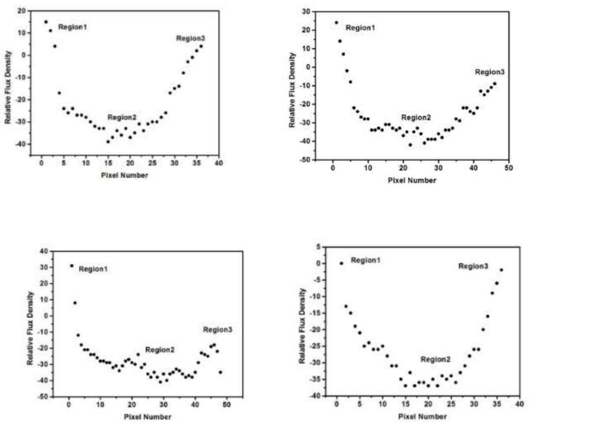

Figure 9: Variation of relative flux density along Line-2, 3, 4 and 5 of figure 6 of Moon (From top left to bottom right). The flux density is measured in each pixel of Lines from top to bottom.

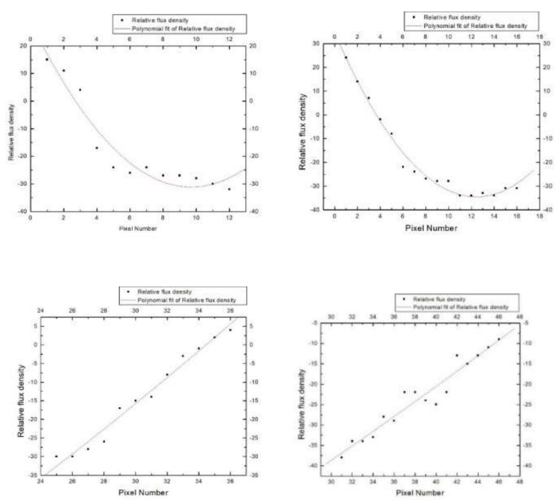

Figure 10: Flux density variation in region 1 along Line-2, 3 with second degree polynomial fit (above). Flux density variation in region 3 along Line-2, 3 with second degree polynomial fit (Below).

$y = 35.23 - 11.41x + 0.468x^2$ with error 2.12, 0.61 and 0.037 , $y = 24.38 - 9.61x + 0.40x^2$ with error 6.22, 1.68 and 0.096 , is $y = 24.38 - 9.61x + 0.40x^2$ with error 6.22, 1.68 and 0.096, $y = 0.59 - 5.56x + 0.268x^2$ with error 2.88, 1.02 and 0.076 in the parameter c, m and a respectively. Similarly, at region 3, the parabolic fit model is $y = -102.84 + 2.35x + 0.018x^2$with error 53.18, 3.52 and 0.058, $y = -68.27 + 0.52x + 0.017x^2$with error 59.49, 3.08 and 0.039, $y = -79.84 + 1.47x - 0.006x^2$with error 121.49, 6.05 and 0.075, $y = 98.33 - 11.19x + 0.234x^2$with error 36.87, 2.44 and 0.04 in the parameter c, m and a respectively.

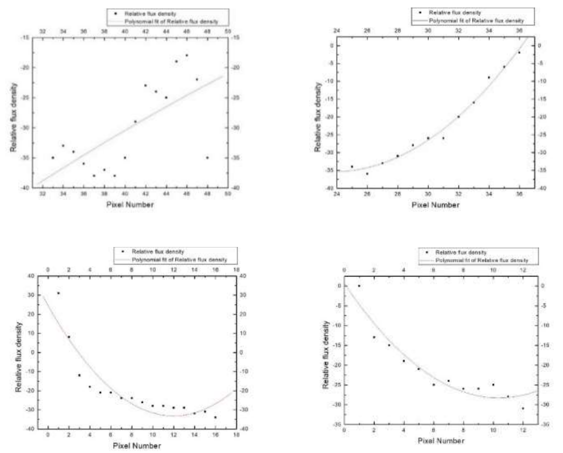

Figure 11: Flux density variation in region 1 along Line-4, 5with second degree polynomial fit (above). Flux density variation in region 3 along Line-4, 5 with second degree polynomial fit (Below).

Results and Discussion

In order to study the variation of relative flux density of the Moon, we had analyzed the figure 4(Blue filter) with the ALADIN2.5 software. The inner-most contour level of the FITS image depicts the maximum total flux density. This is due to the projection effect, which means that the image we got with the telescope is a two-dimensional projection of a three-dimensional real object. In the FITS image, we will draw five lines through the center and record the flux density of each pixel along each line. This flux density is denoted by $F_T$in the table 4 and 5. This radiation flux should be resolved using background fluxdensity (F_B)which will be explained further below.

The average value of the relative flux density per pixel that is observed in the field of view, captured in the image is called Background Count. While calculating the flux density of a particular celestial bodies (i.e. Moon in our case), we need to subtract the background flux of other celestial bodies[17]. By clicking oneach of the pixel in the entire field of view,background flux can be obtained from the outer surface of the lowestcontour level of a FITS image.The calculation of background count is shown in thefigure5. Eachtagging(+) sign indicates a single pixel from which the background count is calculated.

Conclusion

We took the FITS images of the lunar surface from 8:00

PM to 10:00 PM, through the telescope by using LPI camera and AUTOSTAR SUITE3.08software. After this, we took one of the best FITS images from the captured collection of FITS images, for the further processing using ALADIN2.5 software. For our research, we had analyzed the figure, FITS images with blue filter, with the ALADIN2.5 software to study the surface flux distribution of the Moon. The relative flux density of the Moon is calculated by comparing its measured flux density (brightness or radio intensity) at a certain wavelength or frequency to a standard or reference value. A dimensionless ratio is often used to express this relative measurement.

We can draw following conclusions after measuring the diameter and height of the craters from National Observatory, Nagarkot.

- The relative flux density at the center region of the lunar surface is nearly constant and maximum. The maximum relative flux density at the center region of the Moon's surface is largely due to direct sun light exposure during the lunar day, effective solar radiation absorption, low albedo (fraction of sunlight reflected by an object or surface), and the absence of an atmosphere that would normally scatter or absorb sunlight. The above factors combine to make the central region of the Moon's surface one of the hottest and brightest spots visible from Earth, thus making the flux density (brightness) maximum at the center region.
- The relative flux density increases from outer region to the inner region, remains nearly constant in the center region, and then again decreases moving towards the outer region. This variation in relative flux density from outer region to inner region may be due to the differences in surface composition and temperature across the Moon's surface. The outer regions of the Moon are characterized by highland areas and mountains composed up of lighter-colored materials such as another site and breccias, which have lower emissivity and reflect more sunlight, resulting in a lower flux density. The inner regions of the Moon, i.e., the near side of the Moon (where most maria are located), are primarily composed of dark, iron-rich basalts, which have higher emissivity and absorb more sunlight, resulting in a higher flux density. The outer regions of the lunar surface often have more rocky and uneven landscape in comparison to the relatively smoother inner or central regions. The variation in surface roughness can affect the amount of sunlight reflected and scattered by the surface, resulting the change in the flux density.
- The variation in relative flux density in the direction of the plateau is not linear and, thus is better characterized by a second order degree polynomial fit.

We believe that this research work will be the threshold work for the future work in the moon from this particular region.

Data Availability Statement

Visual flux collected by Meade 16-inch LX200GPS Schmidt-Cassegrain telescope from the National Observatory Nagarkot, Nepal. All data will be available upon request from corresponding author.

Acknowledgements

We have great pleasure to B.P. Koirala Memorial Planetarium, Observatory and Science Museum Development Board, Executive Director and all the staffs for their generous co-operation in carrying the data for conducting this work. One of the authors acknowledges Department of Physics, Amrit Campus, Tribhuvan University, Nepal.

References

1. https://solarsystem.nasa.gov/moons/earths-moon/overview/ (viewed on 11th and 12thMay, 2025).
2. https://planetary.s3.amazonaws.com/web/assets/pictures/moon nearside-farside.jpg (viewed on 11 May, 2025).
3. https://www.britannica.com/place/Moon(viewed on 11May, 2025).
4. https://solarsystem.nasa.gov/moons/earths-moon/in-depth/ (viewed on 11 May, 2025).
5. https://www.bbc.com/news/articles/cyv183v02j3o (Viewed on 10th April 2026)

6. Shkuratov, Y, Kaydash, V., Korokhin, V., Velikodsky Y, Opanasenko N. and Videen G. 2011. Optical measurements of the Moon as a tool to study its surface. *Planetary and Space Science.* **59**(13): 13261371. Doi:https://doi.org/10.1016/j.pss.2011.06.011
7. Oberst, J., Christou, A. R., Moser D. and Wagner. 2012. The present-day flux of large meteoroids on the lunar surface-a synthesis of models and observational techniques. *Planetary and Space Science*.**74** (1): 179 - 193. Doi: https://doi.org/10.1016/j.pss.2012.10.005
8. Forgan D. H., Mead , A., Cockell C. S. and Raven, J. A. 2014.Surface flux patterns on planets in circumbinary systems, and potential for photosynthesis. *International Journal of Astrobiology*. **14**(3): 465-478.
9. Heinken ,G. H., Vaniman, D. T. and French, B. M. 1991. *Lunar Sourcebook*: *A User's Guide To Moon.*Cambridge University Press, Cambridge, UK.
10. Acharya, U. 2017.*Astrophotography To Study Lunar Features And Determination Of Size Of Craters*. M.Sc. Dissertation. Department of Physics, Amrit Campus. Tribhuvan University. Kathmandu. Nepal.
11. https://myearthscience.com/astronomy/the-moon/ (viewed on 11 May, 2025).
12. https://www.interlochenpublicradio.org/2022-06-13/on-strawberri-es-moon-and-stars-this-week-on-the-storytellers-night-sky (vie-wed on 11 May, 2025).
13. Stooke ,P. J. and Tatum, J. B. 2006. Encyclopedia Of Planetary Sciences, edited by J. H. Shirley, R. W. *Fairbridge, Springer Dordrech*. **1**:154-159.
14. Operating Manual: 8", 10", 12", 14", 16" LX200GPS Schmidt-Cassegrain Telescopes, Meade Instruments Corporation, (2003).
15. Operating Manual: Meade LPI Camera Program, Meade Instruments Corporation, (2003).
16. .https://www.techtarget.com/searchstorage/definition/charge coup-leddevice (viewed on 11 May, 2025).
17. https://www.nasa.gov/feature/jpl/nasa-moon-mission-shares insig-hts into-giant-impacts (viewed on 12 May, 2025).
18. https://optcorp.com/products/meade-16-acf-lx200-telescope-wgia-nttripod?srsltid=AfmBOor9N8CKXfZ6PVjcJzIz7AAwXbD6RdnG4PAFInFjQQ-wACnHQFn1).(Viewed on 26 May,2025).
19. Parajuli, P. 2014. *Study Of Different Craters Of Moon Using Meade 16-Inch Schmidt-Cassegrain Telescope*. M.Sc. Dissertation. Department of Physics, St. Xavier College, TribhuvanUniversity. Kathmandu. Nepal.